Earthquake Science
地震学报英文版 ISSN 1674-4519 CN 11-5695/P

Shear wave velocity model using HVSR inversion beneath Bandar Lampung City

Ahmad Zaenudin, Alhada Farduwin, Gede I Boy Darmawan, Karyanto

Citation: Zaenudin A, Farduwin A, Darmawan GIB, Karyanto (2024). Shear wave velocity model using HVSR inversion beneath Bandar Lampung City. *Earthquake Science*, **37**(4): 337–351, doi: 10.1016/j.eqs.2024.04.004

View online: http://www.equsci.org.cn/article/doi/10.1016/j.eqs.2024.04.004

Related articles that may interest you

Near–surface structure from ambient–noise tomography and horizontal–to–vertical spectral ratio beneath the Nankou–Sunhe fault

Earthquake Science. 2020, 33(5–6), 232 https://doi.org/10.29382/eqs–2020–0232–01

Stepwise joint inversion of surface wave dispersion, Rayleigh wave ZH ratio, and receiver function data for 1D crustal shear wave velocity structur

Earthquake Science. 2017, 30(5–6), 229 https://doi.org/10.1007/s11589–017–0197–0

Shallow velocity structure of the Luoyang basin derived from dense array observations of urban ambient noise

Earthquake Science. 2018, 31(5–6), 252 https://doi.org/10.29382/eqs–2018–0252–5

S–wave velocity structure in Tangshan earthquake region and its adjacent areas from joint inversion of receiver functions and surface wave dispersion

Earthquake Science. 2020, 33(1), 42 https://doi.org/10.29382/eqs–2020–0042–05

Estimating the site effects in Luoyang basin using horizontal–to–vertical spectral ratio method from a short–period dense array

Earthquake Science. 2018, 31(5–6), 272 https://doi.org/10.29382/eqs–2018–0272–7

Crustal and upper mantle structure beneath Abaga area in Inner Mongolia revealed by Rayleigh–wave phase velocity tomography

Earthquake Science. 2019, 32(5–6), 207 https://doi.org/10.29382/eqs–2019–0207–03

Follow Earthq Sci WeChat public account for more information

Earthquake Science 37 (2024) 337–351

Contents lists available at ScienceDirect

Earthquake Science

Journal homepage: https://www.keaipublishing.com/en/journals/earthquake-science/

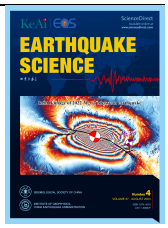

Article

Shear wave velocity model using HVSR inversion beneath Bandar Lampung City

Ahmad Zaenudin[1,✉], Alhada Farduwin[2], Gede I Boy Darmawan[1,2] and Karyanto[1]

[1] *Department of Geophysical Engineering*, *University of Lampung*, *Bandar Lampung* 35145, *Indonesia*
[2] *Department of Geophysical Engineering*, *Sumatera Institute of Technology*, *South Lampung* 35365, *Indonesia*

Key points:

- The study found stiff soil layers at depths of approximately 5 m with a value of v_S < 330 m/s, and bedrock layers with a velocity of over 1250 m/s were visible at a depth of 100 m beneath Bandar Lampung city.
- The city of Bandar Lampung is divided into two zones based on the v_S structure, with a trending NW-SE boundary.
- The north-central-eastern part has higher v_S values and is dominated by hard rock, whereas the south-central-western part has low-to-moderate v_S values and is a groundwater basin area with a thick sediment layer.
- Fault structures are clearly visible in both the lateral and vertical sections, indicating a complex fault structure throughout the city.

A B S T R A C T

The horizontal-to-vertical spectral ratio (HVSR) method has been used to characterize site-effect parameters that are indispensable in seismic hazard and risk-reduction studies in urban areas and rapid land-use planning. This method is widely used because it is the cheapest and simplest geophysical method for the acquisition and processing stages. In subsequent developments, the HVSR method has been widely used to determine elastic rock parameters, particularly shear wave velocity (v_S), through the HVSR curve inversion process. Furthermore, the v_S structural model can be used to delineate the presence of complex geological structures, particularly faults and sedimentary basins. Bandar Lampung is a city in Lampung Province with many fault structures and groundwater basins to the south. There are 83 HVSR measurement points around Bandar Lampung for delineating the presence of fault structures and groundwater basins. We produced the HVSR curve from the measurement results and then performed an inversion process using the particle swarm optimization algorithm to obtain v_S for the depth profile. Subsequently, from this profile, we produced a two-dimensional (2D) lateral and vertical model. The mean v_S value was calculated from all the measurement points, and we found stiff soil layers reaching depths of approximately 5 m, with a value of v_S < 330 m/s. A bedrock layer with a velocity exceeding 1 250 m/s was visible at a depth of 100 m. Based on the 2D model, the v_S structure shows that the city of Bandar Lampung is divided into two zones, with a NW-SE boundary. The north-middle-eastern part of the city consists of harder rocks. This harder rock is characterized by extremely high v_S values, starting from a depth of 50 m. In contrast, the south-middle-west exhibits a low-moderate v_S anomaly associated with groundwater basins SW

Production and Hosting by Elsevier on behalf of KeAI

© 2024 The Authors. Publishing services by Elsevier B.V. on behalf of KeAi Communications Co. Ltd. This is an open access article under the CC BY license (http://creativecommons.org/licenses/by/4.0).

✉ **Corresponding author.** Zaenudin A, email: ahmad.zaenudin@eng.unila.ac.id

Article history:
Received 9 June 2023
Received in revised form 25 September 2023
Accepted 29 September 2023
Available online 18 December 2023

https://doi.org/10.1016/j.eqs.2024.04.004

of the city. From the 2D v_S structural model, fault structures can be found along the city, characterized by a contrast of v_S values from low to medium and from medium to high.

Keywords: shear wave velocity; HVSR; fault structures; groundwater basin; Bandar Lampung City

Citation: Zaenudin A, Farduwin A, Darmawan GIB and Karyanto (2024). Shear wave velocity model using HVSR inversion beneath bandar lampung city. Earthq Sci **37**(4): 337–351, doi: 10.1016/j.eqs.2024.04.004.

1. Introduction

Site characterization is a powerful tool that provides information on basic seismic risk and describes boundary zones vulnerable to the effects of local earthquakes. Information obtained from site characterization includes fundamental frequency (f_o), site amplification (A_o), and shear wave velocity (v_S). This information is essential for planning strategies for seismic risk mitigation by subdividing potentially earthquake-prone areas into zones based on the same geological and geophysical properties. Thus, seismic responses can vary inside urban settlements owing to lateral and vertical heterogeneities in the geologic setting (Hartzell et al., 1997; Panzera et al., 2017; Toni et al., 2019). In areas with complex geologic settings, where manufactured structures interfere with the reconstruction of the subsoil geometry, a detailed geologic survey coupled with knowedge of shear wave velocity and fundamental frequency is important (Panzera et al., 2019). In addition, it is crucial to evaluate the quantitative seismic risk and estimate the site amplification factors precisely because the effect of site amplification is significant, particularly at sites with thick and soft sediments where most urban environments have been built (Kawase et al., 2019).

Local site conditions play a fundamental role in earthquake damage distribution and refer to the effects of the local geological surface and subsurface structure characteristics on seismic ground motion. The seismic ground response is related to the sediment depth (h) and shear wave velocity (v_S) (Aki and Richards, 2002; Stanko et al., 2017), expressed by the fundamental/natural frequency and site amplification of the sediment. A low fundamental frequency indicates thick sedimentary layers and an extremely soft material. For thin sedimentary layers, the fundamental frequency is high. Local site amplification refers to the amplitude increase in seismic wave propagation through surface geological structures. The peak amplitude (A_o) is related to the contrast impedance between the surface layer and underlying bedrock, lateral heterogeneities, material damping of the sediment, and characteristics of the incident wavefield.

Studies using ambient noise measurements (microtremors) have been widely conducted using the horizontal-to-vertical spectral ratio (HVSR) technique. It provides reasonable estimates for determining the natural frequency of soil (Mucciarelli and Gallipoli, 2001). The HVSR method can be applied to various scientific disciplines, including geology (Mantovani et al., 2018), seismology and site micro-zonation study (D'Amico et al., 2008; Gallipoli et al., 2019; Paolucci et al., 2015; Scherbaum et al., 2003), engineering (Mucciarelli and Gallipoli, 2001), fault and subsoil investigations (Akkaya, 2015; Akkaya and Özvan, 2019; Harutoonian et al., 2013; Khalili and Mirzakurdeh, 2019; Maresca et al., 2018; Setiawan et al., 2018; Zaenudin et al., 2022), and archaeology (Abu Zeid et al., 2016, 2017a, b; Bignardi et al., 2017; Wilken et al., 2015).

HVSR applications in the geotechnical field have also been developed to obtain a one-dimensional (1D) layer model described in the shear wave velocity-to-depth profile (Raptakis and Makra, 2010). This shows that the HVSR is sufficient for obtaining the shear wave velocity structure model at a local site. However, if a priori information is known, such as the range of v_S and thickness of the layers around the research area, the accuracy of the HVSR curve inversion increases (Fäh et al., 2003). Several other geophysical methods have been used to determine the thickness and number of layers in the HVSR curve inversion process (Pilz et al., 2010; Maghami, 2021; Rahman et al., 2016; Pamuk et al., 2017).

In this study, the shear wave velocity structure in Bandar Lampung, located in Lampung Province (southern Sumatra Island), was investigated. Bandar Lampung has a relatively complex geological structure, with many fault structures crossing the city and various rock formations. Most of the fault structures are northwest-to-southeast (NW-SE) (Figure 1). Therefore, this study focused on mapping the structure of v_S and estimating the presence of faults from the v_S cross sections. In addition, this study focused on the thickness of the sediment layer in Bandar Lampung. According to Zaenudin et al. (2020), gravity data show that the southwestern area toward Mount Betung contains a thick layer of sediment. In this area, the groundwater basins are located at a depth of 800 m.

Microtremor data obtained using the HVSR method were used to determine the seismic site characteristics (dynamic properties) of subsurface soil layers, expressed

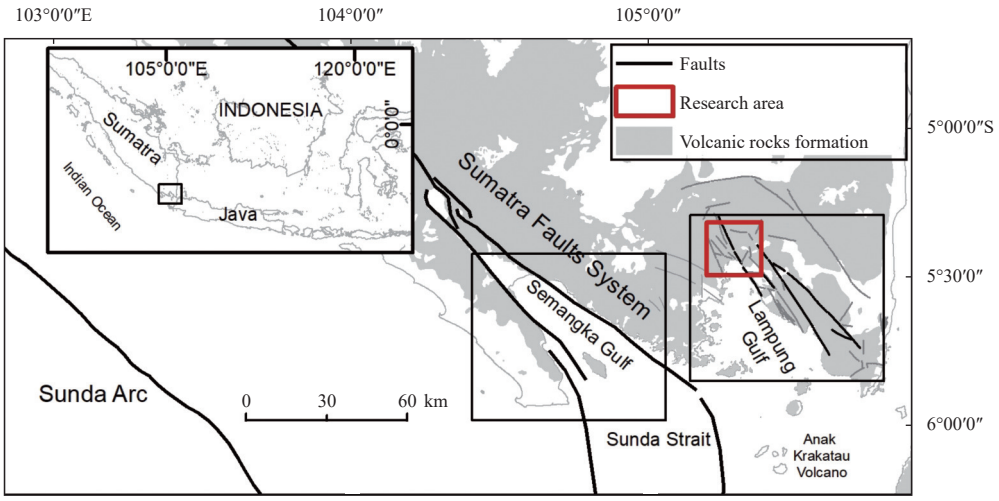

Figure 1. Regional geological structure of the Sumatra fault system along the Semangka and Lampung segment (Barber et al., 2005; Darmawan et al., 2021; Mangga et al., 1993). The red box indicates the research area located in Bandar Lampung City.

by the fundamental/natural frequency (f_o). Then, we inverted the HVSR curve to obtain v_S for the depth profile around Bandar Lampung. In the inversion stage, we used the particle swarm optimization (PSO) inversion algorithm because this method converges quickly and is relatively stable (Farduwin and Yudistira, 2021). Although there are many sophisticated and reliable inversion algorithms for HVSR curve inversion, the inversion method using the PSO algorithm is sufficient for identifying subsurface structures. Using the PSO inversion algorithm, Zaenudin et al. (2022) determined the local fault structure based on the v_S structure obtained from the HVSR curve inversion. To increase the best model of the obtained inversion results, we correlated them with the natural frequency (f_o) as a reference to estimate the thickness of the sediment layer and depth of the bedrock, as suggested by Ibs-von Seht and Wohlenberg (1999).

2. Geological setting

The study area is located on the southern tip of Sumatra Island in the southern part of Lampung Province. Sumatra is one of the largest islands in Indonesia, with complex geological conditions. The structure of the island resulted from the subduction of the Indian Plate beneath the Eurasian Plate. This subduction has occurred since the Cenozoic Period, forming a subduction zone along the collisional boundary (McCaffrey, 2009) and causing a changing the position of Sumatra Island, which initially trended west-east to NW-SE (Hamilton, 1979). These conditions make Sumatra an area of high seismicity. The deformation process on Sumatra began during the Oligocene-Miocene. This led to the formation of the Sumatra Fault, which is a horizontal fault that remains active today and forms several fault segments (Barber et al., 2005). The Sumatra Fault extends from Aceh (northern tip of Sumatra) to Lampung (southern tip) and is a dextral strike-slip fault that moves obliquely to the northwest (Sieh and Natawidjaja, 2000).

Regionally, the study area lies within the Sumatra fault system segment, extending from the pull-apart basin zone in Suoh to the Semangka and Lampung Bay segments. The Semangka fault represents the Semangka Bay segment. It continues to the Sunda Strait, whereas the Lampung-Panjang and Tarahan faults represent the Lampung Bay segment and continue to the Rajabasa Mountains. Sinistral strike-slip faults dominate the fault segment around Lampung Bay. This fault movement is greatly influenced by the oblique subduction of the Eurasian Plate in the Sunda Arc.

Bandar Lampung is located 80 km (western research area) from the Semangka Fault earthquake source line. The Lampung-Panjang and Tanjung-Karang faults are also located in this city with the same orientation and characteristics as the Semangko Fault. Based on the geological map of Tanjung Karang (Mangga et al., 1993), Bandar Lampung consists of three main strata (Figure 2): The Pre-Tertiary consisting of the bedrock of metamorphic rock (basement of Bandar Lampung) is distributed in eastern and southeastern research area, and intrusive igneous rock is distributed in the eastern area; the Tertiary strata are composed of the magmatic intrusive igneous rock in the western part and sedimentary rock in the southeastern-northeastern and western-southwestern parts; and the Quaternary strata are composed by sedimentary rock, surface deposits (alluvium), and young volcanic

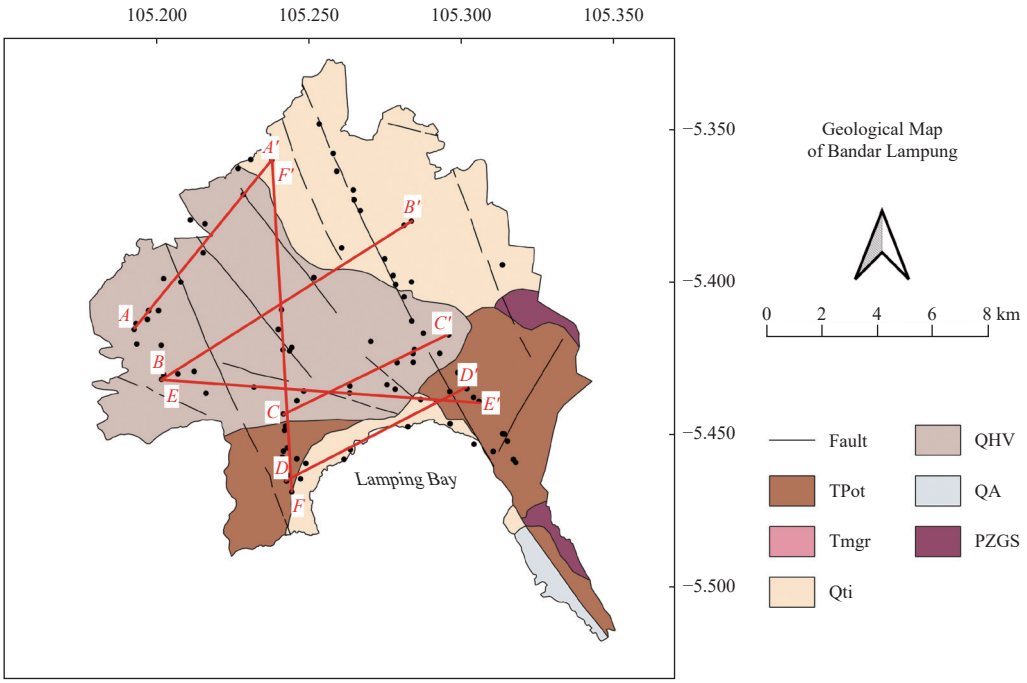

Figure 2. Geological map of Bandar Lampung consisting of surficial deposits (QA: cobbie, pebble, sand, clay, and peats), volcanic rock (QHV: andesite-basalt lava, breccia, and tuff; Qti: pumiceous tuff, rhyolitic tuff, welded tuff, tuffaceous claystone, and tuffaceous sandstone), sedimentary rock (Tpot: welded tuff and breccia with intercalations of chert), metamorphic rock (PZGS: green amphibole-schist and dioritic orthogneiss amphibolites), and intrusive rock (Tmgr: granite and granodiorite). The red lines indicate the trajectory of cross sections *A* to *F* and the black dots are HVSR acquisition points (modified from Mangga et al., 1993).

deposits distributed in the part of central to the western research area.

Bandar Lampung contains four geomorphological units: structural, volcanic, denudational, and fluvial (Mulyasari et al., 2019). The structural unit is associated with the Lampung-Panjang and Tanjung-Karang faults, which played a role in the changing geomorphology. The volcanic unit was controlled by recent volcanic activity (Betung Volcano) and magnetism. Denudational units were controlled by erosion and are characterized by a lithology or rock formation on a hill morphology that differs from the surrounding lithology. Fluvial units are the products of recent geological processes. They are characterized as unlithified and sedimentary materials distributed in a plain or flat relief (Rustadi et al., 2022).

3. HVSR theory

HVSR is a method based on ambient seismic noise measurements. Ambient noise, commonly called microtremors, can appear anywhere on the surface of the Earth and is related to atmospheric phenomena and anthropogenic activities (Asten, 1978; Gutenberg, 1958). A microtremor is characterized by tiny wave oscillation (10^{-4} to 10^{-2} mm) with highly attenuated spectral components and can be measured by passive recording techniques. During propagation from source to receiver, elastic waves encounter attenuation—generally caused by geometric factors (increased wavefront dimensions)—and are inelastic because not all rocks are perfectly elastic, particularly sediments.

The HVSR method is simple and reliable, estimating natural/dominant frequency values by measuring the three components of microtremors (NS, EW, and vertical). Owing to its simplicity in measurement and processing, this method has developed rapidly. It has been widely applied in many areas to determine site effects and microzonation maps, particularly in densely populated areas (urban settlements). This method was first proposed by Nogoshi and Igarashi (1970, 1971), then developed by Nakamura (1989), and is commonly referred to as the Nakamura Technique. In 1989, Nakamura stated that the peak amplitude of the HVSR was the result of multiple body-wave reflections. Nevertheless, Nakamura (2000) revealed a theory stating that there is a combination of surface and body waves that affects the shape of the HVSR curve and depends on the viscoelastic parameters of the layers, distance, and distribution of sources (Sylvette et al., 2006).

The HVSR processing stage obtains an HVSR curve at a single point in the measurement location. The three

recorded seismic components are divided into several windows based on the desired window length. Then, on each of these windows, a Fourier transform is performed for all components, smoothing the curves, and calculating the ratio between the horizontal and vertical components. The Fourier spectral ratio between the horizontal and vertical (H/V) components of the microtremors can be expressed as

$$H/V(\omega) = \left\{\left[S^2(\omega)_{\mathrm{NS}} + S^2(\omega)_{\mathrm{EW}}\right]/2S^2(\omega)_{\mathrm{V}}\right\}^{1/2}, \quad (1)$$

where $[S(\omega)_{\mathrm{NS}}$ and $S(\omega)_{\mathrm{EW}}]$ are the spectra of two horizontal components, $[S(\omega)_{\mathrm{V}}]$ is the spectrum of the vertical component (V), and ω is the angular frequency. The average value was calculated from all curves to obtain the HVSR curve as a function of frequency. The HVSR curve consists of one or more peaks describing the subsurface layer as several layers of sediment above the bedrock layer. In general, we assume that there is more than one peak amplitude in the HVSR curve. In this case, the peak with the lowest frequency is called the resonant fundamental frequency (f_{o}).

There are two types of parameters at the peak of the curve: the peak amplitude and frequency. The peak frequency, where the peak amplitude occurs, is referred to as the natural or fundamental frequency (f_{o}). In contrast, the peak amplitude (A_{o}) is directly related to the speed contrast, i.e., a sharp speed contrast produces a large H/V peak amplitude and vice versa. The peak amplitude in the HVSR curve is also caused by the difference between the top layer of the sediment and the rock layer below it (SESAME, 2004). The HVSR method is suitable for areas with low-to-moderate seismic activity (Kyaw et al., 2015).

4. Methodology

Microtremor measurements were conducted in Bandar Lampung City using a three-component seismometer at 83 measurement point locations (Figure 2) for 25–30 min with a sampling time of 0.01 s. Determining the measurement parameters was necessary to reduce the disturbance at the measurement location. We used a Butterworth filter of order two with a cutoff frequency of approximately 0.3 Hz to reduce the effect of wind around the measurement location and drift caused by the tool (Mihaylov et al., 2016, 2019). During processing, we used *Geopsy* and *Octave software* concerning the standard HVSR processing procedure to obtain a reliable curve (Nakamura, 1989; SESAME, 2004). The processing parameters include a frequency filter range of 0.5–20 Hz and window length of 30 s with 25% overlap. (Maghami et al., 2021). We then applied an antitrigger algorithm to eliminate transient or very low amplitude signals (short-term average (STA)=1 s; long-term average (LTA)=30 s) with STA/LTA of 1.0–3.5. We used a filter with a smoothing coefficient of 20 to remove the effects of modulation and spikes with extreme values on the HVSR curve (Konno and Ohmachi, 1998). The following equation is used to calculate the HVSR curve for each window:

$$\mathrm{HVSR} = \frac{H(f)}{V(f)},$$
$$H(f) = \sqrt{E(f)^2 + N(f)^2}, \quad (2)$$

where $H(f)$ = amplitude spectra of the horizontal component; $V(f)$ = amplitude spectra of the vertical component; $E(f)$ = amplitude spectra of EW component; $N(f)$ = amplitude spectra of NS component;

The spectral ratio between the horizontal and vertical components of ambient noise shows a peak value at a certain frequency, which is related to the resonant frequency (f_{o}) of the soil layer thickness at a site (Ibs-von Seht and Wohlenberg, 1999):

$$h = a f_{\mathrm{o}}^{b} \quad (3)$$

where h is the depth of the sediment layer (Quaternary), and a and b are the correlation coefficients related to the geometry and geotechnical properties of a site. From Equation (3), it is difficult to determine the suitability of the correlation coefficient for the geometry of the dynamic properties of the soil layers. Therefore, the HVSR curve inversion was used to determine the thickness of each layer at each site.

In the HVSR curve inversion stage, we applied the PSO algorithm to estimate the value of the shear wave velocity (v_{S}) against depth (H). This algorithm has advantages in terms of geophysical data inversion because it converges quickly and is relatively stable (Farduwin and Yudistira, 2021; Farduwin et al., 2021). Zaenudin et al. (2022) compared the PSO and GA algorithms using synthetic modelling and found that PSO is faster, provides the best solution, and is more stable. PSO is an inversion technique that imitates the social behavior of bird swarms (particles or individuals) to find food (Kennedy and Eberhart, 1995). Flocking behavior and individual intelligence affect the behavior of each particle in finding food or a target. When an individual finds the closest target, all others head toward it.

There are five stages in the PSO algorithm. First, we determine the number of individuals to generate the search space of the model parameter (where $\boldsymbol{X}_{\mathbf{min}} \le \boldsymbol{X} \le \boldsymbol{X}_{\mathbf{max}}$). The second stage generates an initial population of $\boldsymbol{X}$ using random numbers in the model parameter search space determined in the first stage. We then obtain the initial

populations $x_1^0, x_2^0, x_3^0, \cdots ., x_j^i$; where i = iteration, j = n-th individual, and n = number of individuals. For the HVSR inversion, the model parameters consisted of h and v_S. The velocity (v) of each individual was set to zero in the initial iteration ($v_1^0 = v_2^0 = v_3^0 = \cdots = v_i^0 = 0$). The third stage involves calculating the objective functions $f[x_1^0]; f[x_2^0]; f[x_3^0]; \cdots; f[x_j^0]$. In this study, we used norm-2 ($\|e\|^2$) to calculate the objective function. In the next stage, we determine parameters l and g, where l is the best position of the individual in the given iteration. Thus, g is the best position that a particle can reach within a group. The best positions l and g, are determined from the smallest objective function ($f_{\min}$). In the final stage, we update the v and x values for each iteration with the following equation:

$$\begin{aligned} v_i(k+1) &= \omega v_i(k) + \varphi_1(g(k) - x_i(k)) + \varphi_2(l_i(k) - x_i(k)), \\ x_i(k+1) &= x_i(k) + v_i(k+1). \end{aligned} \tag{4}$$

where

$$\varphi_1 = r_1 a_g, \varphi_2 = r_2 a_l, r_1, r_2 \to (0,1)\, \omega, a_l, a_g \in \mathbb{R} \tag{5}$$

ω is the inertia moment, φ_1 and φ_2 are the global and local acceleration, and a_l and a_g are global and local acceleration constants. Using regressive discretization (RR-PSO) on v and a in the time function (Fernández-Martínez and García-Gonzalo, 2012), we obtain a discrete model using the following equation:

$$\begin{aligned} x^{'}(t) &\simeq \frac{x(t) - x(t-\Delta t)}{\Delta t}, \\ x^{''}(t) &\simeq \frac{x(t) - 2x(t-\Delta t) + x(t-2\Delta t)}{\Delta t^2} = \frac{x^{'}(t) - x^{'}(t-\Delta t)}{\Delta t}. \end{aligned} \tag{6}$$

Then, we apply the following relationship,

$$\begin{aligned} & x(t) = (x(t-\Delta t) + v(t)\Delta t, \\ & \frac{v(t) - v(t-\Delta t)}{\Delta t} + (1-\omega)\, v(t) + \varphi(x(t-\Delta t) + v(t)\,\Delta t) = \varphi_1 g(t-t_0) + \varphi_2 l(t-t_0), \\ & v(t) = \frac{v(t-\Delta t) + \varphi_1 \Delta t(g(t-t_0) - x(t-\Delta t))}{1 + (1-\omega)\,\Delta t + \varphi \Delta t^2} + \frac{\varphi_2 \Delta t(l(t-t_0) - x(t-\Delta t))}{1 + (1-\omega)\,\Delta t + \varphi \Delta t^2}. \end{aligned} \tag{7}$$

Then, the equation for RR-PSO can be written as follows:

$$\begin{aligned} v(t-\Delta t) &= \frac{v(t) + \varphi_1 \Delta t(g(t) - x(t)) + \varphi_2 \Delta t(l(t) - x(t))}{1 + (1-\omega)\,\Delta t + \varphi \Delta t^2} \\ x(t+\Delta t) &= x(t) + v(t+\Delta t)\,\Delta t; t, \Delta t \in \mathbb{R} \\ x(0) &= x_0; v(0) = v_0; \varphi = \varphi_1 + \varphi_2. \end{aligned} \tag{8}$$

In the inversion stage, five-to seven-layer models were used. Seven layers were used at points located on the boundaries of the three rock formations, and there are many fault structures in the area. This method is expected to image a more detailed subsurface model because of its complex structure. We limited the search space for the v_S model in layer 1 to 100–800 m/s, 2–4 to 500–1 500 m/s, and 5–7 to 800–2 500 m/s. This search space refers to the EC8 soil classification (European Commission, 2004) where soil deposits with loose-to-medium cohesion values or soft-to-hard soil layers have v_{S30}<180 m/s. We assumed that the v_S value had the same range as that v_{S30}; therefore, we limited the search space to a minimum of 100 m/s. The maximum value was set to 800 m/s because dense sand, gravel, or clay deposits do not exceed 800 m/s. Furthermore, we set a larger value for the downward layer assuming that the velocity increases with depth. Therefore, we set the velocity to 2 500 m/s for the last layer.

In search space model h, we created several schemas. For this model, the search space for layers 1–3 ranged from 1 to 20 m and that for layers 4–7 ranged from 5 to 50 m. We developed this scheme to detect thin layers associated with near-surface sediment layers. Then, we assigned each layer fixed q_p and q_s values of 30 and 10, respectively. We estimated the P-wave velocity (v_P) and density (ρ) values using the following equation (Brocher, 2005):

$$v_P = 0,9409 + 2,0947 v_S - 0,8206 v_S^2 + 0,2683 v_S^3 + 0,0251 v_S^4 \tag{9}$$

$$\rho = 1,6612 v_P - 0,4721 v_P^2 + 0,0671 v_P^3 - 0,0043 v_P^4 + 0,000106 v_P^5 \tag{10}$$

where v_P is in km/s and density is in g/cm^3. Equation 4 is valid for v_S values of 0–4.5 km/s. The uncertainty information was calculated using the standard deviation of all models produced during the inversion process. The forward function used in this inversion stage is from Herak (2008), who assumes that the 1D model of the HVSR curve depends only on the ground response (amplification spectra) owing to the vertical propagation of body waves. Although several researchers have used the surface wave approach—particularly Rayleigh wave ellipticity—and more complex modeling using Rayleigh and Love waves and the full wavefield approach, both comprehensive approaches used full wavefields or body waves to produce similar (but not identical) curves (Albarello et al., 2023). The only difference was in amplitude (H/V).

5. Results and discussion

5.1. Dominant frequency (f_0)

The dominant frequency value was selected

automatically using *Geopsy software,* which was selected at the peak of the HVSR curve. Figure 3 shows the dominant frequency values, ranging from 0.9 to 7 Hz. Based on the figure, the Bandar Lampung area is regionally dominated by relatively moderate-to-high f_o values (f_o > 2 Hz), where high f_o anomalies appear at the northern, southern, and western ends and in the central part to the east of Bandar Lampung City. The high f_o anomaly in the city center correlates with young volcanic deposits (QHV) consisting of andesite-basalt lava, breccia, and tuff. This young volcanic deposit originated from Mount Betung to the west. In addition, a low f_o anomaly was observed in several parts of the city center, including the SW-central region, several parts above the NE, and the NW-central-SE direction. These low f_o anomalies were primarily correlated with sedimentary deposits (TPOT and QTI) with tuff-dominated lithology. Areas with low f_o values indicate that the area is composed of soft soil and has a thick layer of sediment. Thus, the sediment layers at the northern, western, and southern ends and central-to-east have a thin layer of sediment compared to other areas. In other words, the dominant frequency value in an area can be correlated with the thickness of the sediment layer. This is consistent with the v_S distribution map shown in Figure 7, in which areas with high frequencies have low v_S values at approximately 30 m depth. The rest, at approximately 100 m, showed relatively high v_S values , which spread from north to east and southeast.

5.2. 1D model of v_S structure from PSO inversion result

In this study, the v_S-to-depth profile was obtained from the PSO inversion algorithm using the Herak (2008) code for the HVSR forward model based on body waves, where the approach using body waves is better than that using surface waves (Dal Moro, 2008; Lunedei and Albarello, 2010). The PSO algorithm was selected because of its quick convergence, stability, and ease of implementation (Ding YM et al., 2019; Fernández Martínez et al., 2010; Pallero et al., 2017). We then used the inversion results to create a v_S distribution map at a certain depth and produced a cross-sectional map that crosses the measurement points in the Bandar Lampung area. A subsurface-layer model with five to seven layers was used for the inversion process. Models with more than five layers were used in areas with complex structures. This was performed to obtain a detailed model describing the fault structure in the Bandar Lampung area.

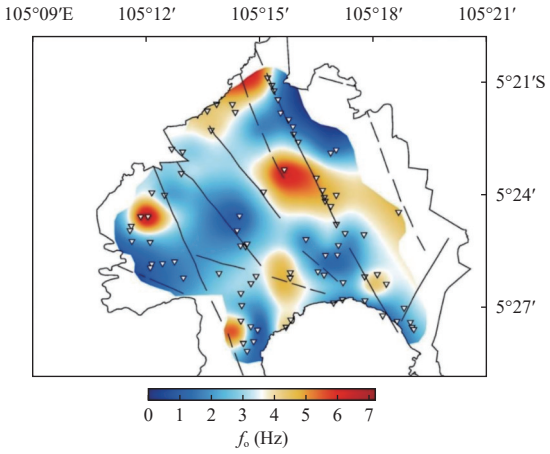

Figure 3. Map of dominant frequency (f_o) around Bandar Lampung City.

Figure 4 shows the HVSR curves obtained at several measurement sites and the one resulting from inversion using the PSO algorithm. The inversion results show a relatively matched HVSR curve between the observed and calculated values. The curve in Bandar Lampung was dominated by wide peak curves, which indicated the possibility of complex variations in the sedimentary and bedrock structures. This is consistent with the geological conditions of Bandar Lampung, where many faults cross in the NW-SE direction. The PJ13 and PJ18 curves showed more than one peak, indicating an impedance contrast at different depths. This is because of the geological conditions at that point, in the form of non-compact sediments on the surface, which are composed of compacted sediments below and extremely compact bedrock layers at the bottom.

Figure 5 shows the subsurface layering model based on the v_S value profile against depth. The results of this inversion model were obtained to 250 m, with an average depth of 150 m. The minimum depth of the inversion results was 100 m. As shown in Figure 5, the distribution of v_S increased with increasing depth. This can also be seen in Figure 6, which shows that velocity v_S increases to a depth of 150 m. v_S increased significantly at depths of 5, 15, 45, and 100 m. At a depth of 0–5 m, the soil was dominated by layers with v_S < 330 m/s, making it a stiff soil. Then, at a depth of 15 m, it started to increase to 430 m/s and continued to increase until its speed reached 800 m/s at a depth of 45 m. At a depth of 100 m, the value of v_S appeared to increase significantly until the speed reached 1 250 m/s, indicating a harder rock layer. The speed increased to 1 350 m/s at a depth of 150 m.

5.3. v_S structure

The v_S distribution map in the subsurface layer of the city of Bandar Lampung shows a clear structural trend. Laterally, v_S showed a relatively significant change and

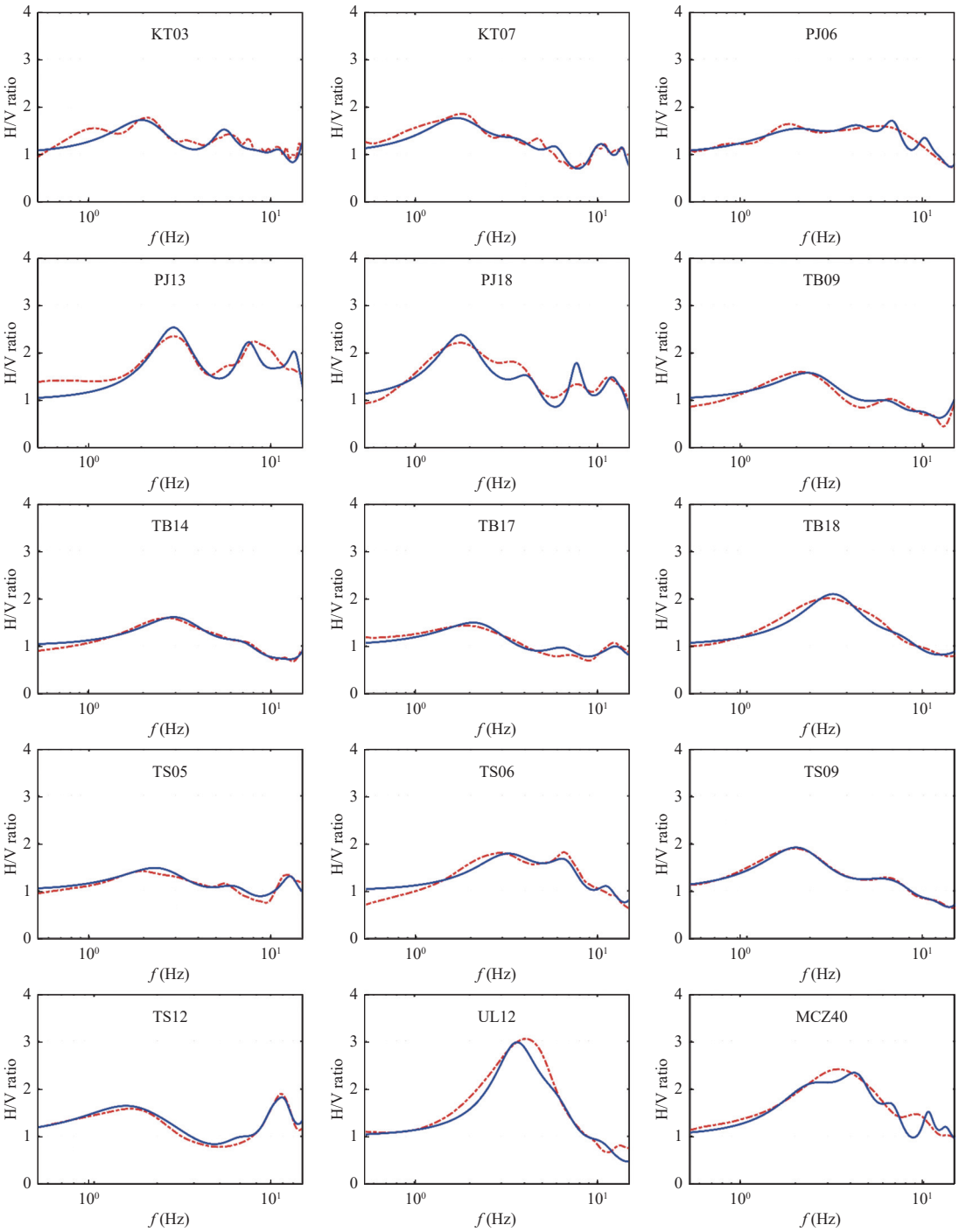

Figure 4. HVSR curve obtained for several observation sites (dashed red line), and the best HVSR curve obtained from the inversion process (blue line).

was marked in areas with faults. This indicates that the fault became the boundary of the changes in v_S, starting from low-to-medium or medium-to-high. v_S can be used to estimate sediment thickness using the well-known quarter-wavelength approximation (Ryanto et al., 2020) or the relationship between the average shear wave velocity and the fundamental resonant frequency. The sediment thickness was not calculated in this study. However, we examined at the distribution of v_S. Figure 7 shows the distribution of v_S at 0, 30, 50, and 100 m. At a depth of 0 m, Bandar Lampung City was dominated by low-to-moderate v_S. Low velocity dominates in most areas, particularly in the north, which has a very low-velocity anomaly. Conversely, there is a moderate velocity at the

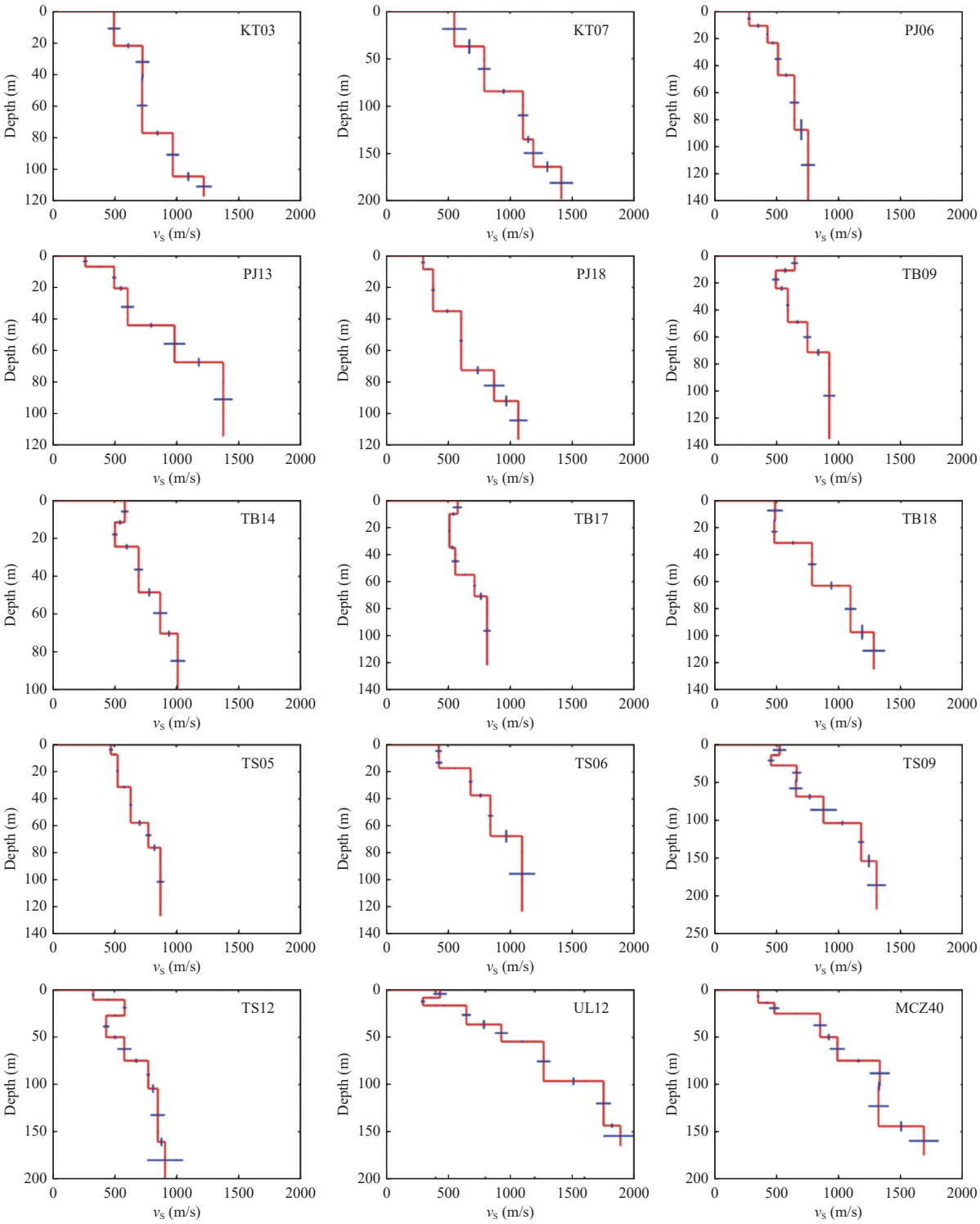

Figure 5. v_S profile obtained from the inversion process using the PSO algorithm. The blue line shows the uncertainty of each layer.

west end toward Betung Mountain and parts of the city center to the east. At a depth of 30 m, the distribution of v_S exhibits a relatively sharp change in the north-central-east direction, where a moderate anomaly (1 000 m/s) appears and is relatively higher than in other areas. This trend continued to 100 m depth. Based on Figure 6b–d, Bandar Lampung City is divided into two parts, where the north-central-eastern part has a higher anomaly. In contrast, the south-central-west region exhibited a relatively moderate anomaly.

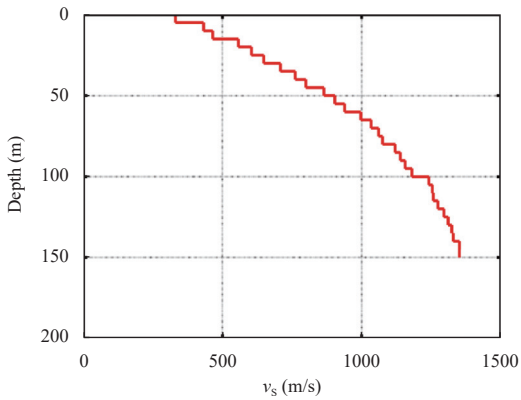

Figure 6. Mean v_S profile around Bandar Lampung City.

The north-central-east area represents a higher anomaly where v_S reaches 2000 m/s. This high anomaly indicates a rock layer that is harder than those in other areas. This corresponds to the f_o distribution map (Figure 3), which shows that the north-central-east area has a high f_o anomaly, indicating that the area has a thin sediment layer. The thickness of the soft sediment layer in this area was estimated to be no greater than 30 m. The west-central-south area shows a relatively low-moderate anomaly (v_S < 1 000 m/s), indicating a relatively thick layer of sediment. This is consistent with the results of Zaenudin et al. (2020), who used the gravity method to identify groundwater basins. The results show that the south-central-west regions have low-to-moderate v_S. These values correlate with the presence of groundwater basins, corresponding to a low residual Bouguer anomaly from a previous study. The zero-value contour of the residual SVD Bouguer anomaly indicates the groundwater basin boundary. From this correlation, it is clear that the low v_S in the area is related to the presence of fluids filling the soil layers; in this case, it is related to the groundwater in the basin.

5.4. v_S cross section

The data processing results showed patterns of v_S that could be interpreted as potential fault-plane boundaries. Three potential fault plane boundaries were successfully interpreted in cross sections *A-A′* and *B-B′* (Figure 8). These fault planes were estimated to be part of the sinistral strike-slip fault of the Lampung-Panjang segment. There is potential for vertical displacement based on the pattern of shear wave velocities greater than 1 000 m/s. Whether this

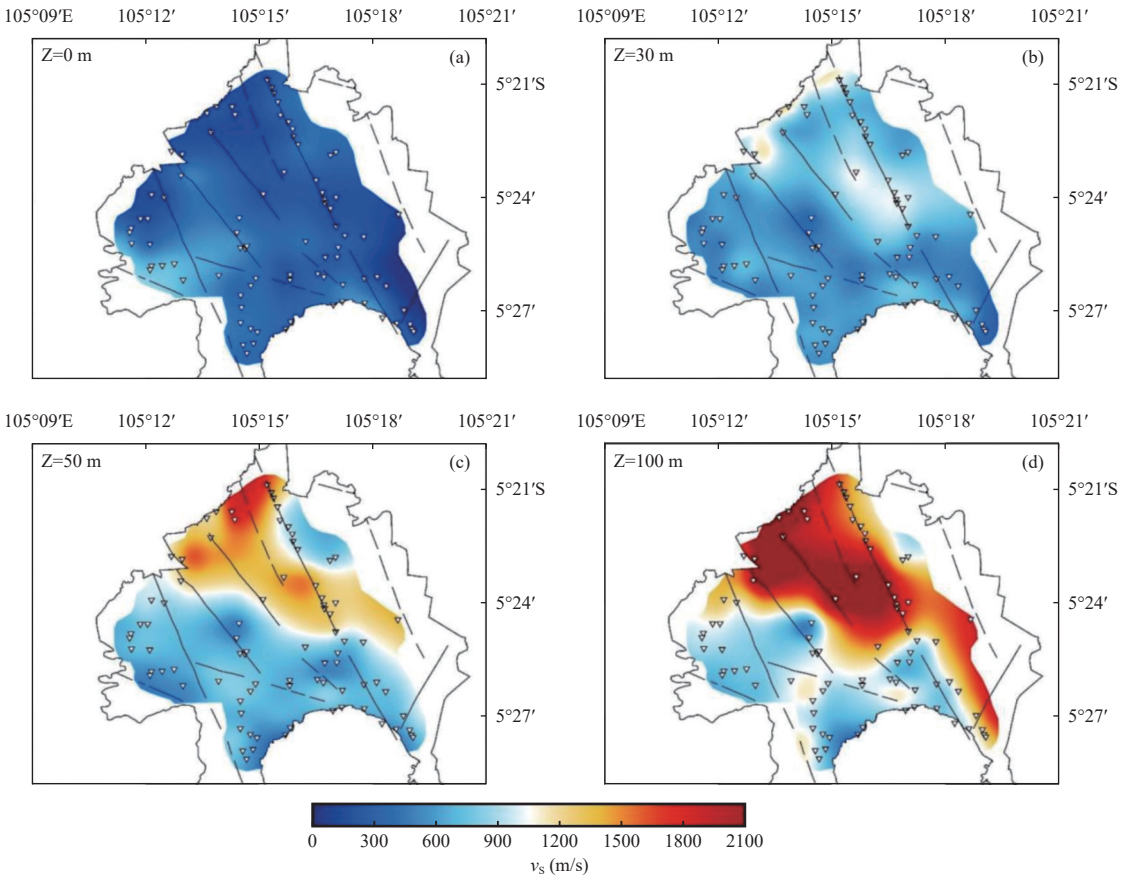

Figure 7. v_S structure of Bandar Lampung city obtained from HVSR inversion at 0 m (a); 30 m (b); 50 m (c); and 100 m (d). The black lines on the map indicate geologically confirmed faults based on the regional geological map.

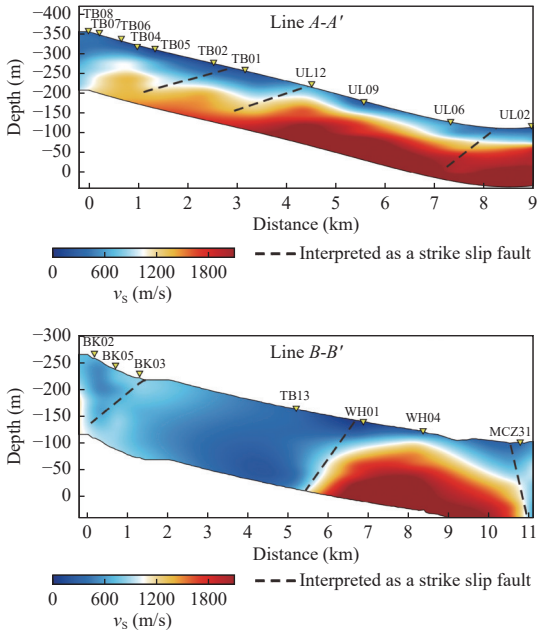

Figure 8. Inverse modeling of cross sections *A-A′* and *B-B′*, indicating the potential for strike-slip fault structures.

indication can be interpreted as oblique movement accompanying a strike-slip fault requires further comparative data. However, this approach is expected to provide preliminary indications that support previous research on structural alignments based on gravity anomalies and second-vertical derivative residual anomalies in Bandar Lampung (Zaenudin et al., 2020).

Interesting results were also obtained from cross-sectional models *C-C′* and *D-D′*, which indicate the potential for strike-slip fault planes, particularly near Lampung Bay. Geologically, this area is a depression located near Paleozoic schist bedrock. Outcrops of this bedrock are influenced by a sinistral strike-slip fault known as the Tarahan fault. The v_S distribution pattern was dominated by velocities of less than 1 000 m/s, identified as Lampung Bay surface deposits. The bedrock is located in deeper areas, with a pattern returning to the surface in the Tarahan area, as shown in cross section *C-C′* of Figure 9. The interpretation of the downward movement of the fault zone also supports the geomorphological conditions of the Tarahan area in Lampung Bay. In addition, the results of the gravity measurements indicate a low-anomaly area in this region that can potentially be a groundwater basin zone (Rustadi et al., 2022; Zaenudin et al., 2020).

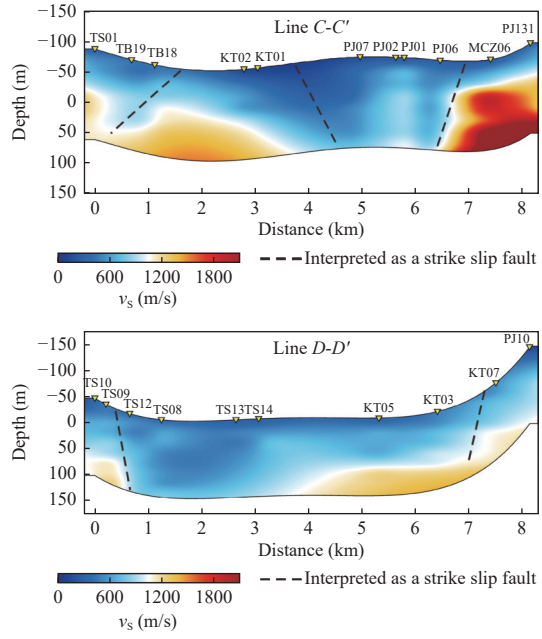

Figure 9. Inverse modeling of cross sections *C-C′* and *D-D′*, indicating the potential for strike-slip fault structures.

The next modeling was conducted on cross sections *E-E′* and *F-F′*, intersecting the previous cross sections in the northwest-southeast and south-north directions, respectively (Figure 10). The shear wave velocity distribution pattern shown in cross section *E-E′* was consistent with those of cross sections *C-C′* and *D-D′*. The potential for strike-slip fault structures was not clearly visible. However, this can still be seen from the pattern shown by velocities above 1 000 m/s. In addition, a potential strike-slip fault pattern indicating vertical movement in the Tarahan fault area was identified at the right end of cross

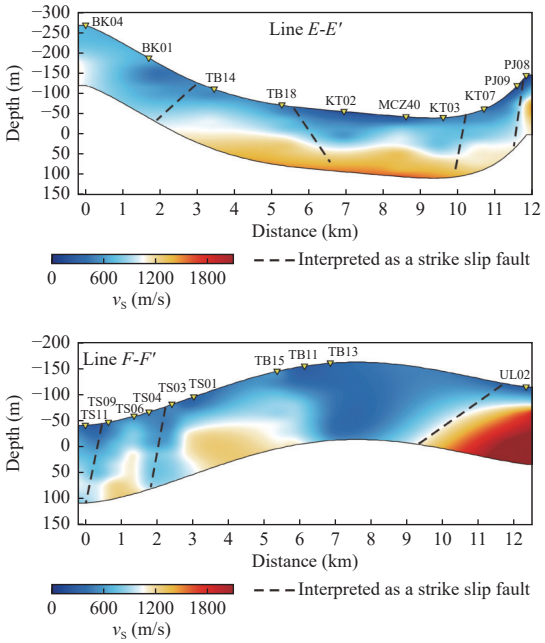

Figure 10. Inverse modeling of cross sections in the northwest-southeast (Line *E-E′*) and south-north directions (Line *F-F′*).

section *E*-*E*′. These velocity patterns were also confirmed from cross sections *C*-*C*′ and *D*-*D*′. Moreover, the shear wave velocity model in cross sections *F*-*F*′ showed a pattern that was consistent with cross sections *A*-*A*′ and *B*-*B*′. The consistency between the shear wave velocity model and previous gravity research results strengthens the interpretation of fault structures. These fault structures limit the potential groundwater basin area in Bandar Lampung (Zaenudin et al., 2020).

6. Conclusions

In this study, the v_S structure in Bandar Lampung City was estimated using microtremor data (natural seismic noise) and the HVSR technique. A total of 83 measurement points were used to detect geological structures and groundwater basins in the southern city, Bandar Lampung. The inversion method used in this study was PSO. This algorithm was selected because it is a global approach that avoids being trapped in a minimum local solution and is relatively fast and stable. In this regard, the v_S structures obtained from the inversion of the HVSR curve are displayed in the two-dimensional (2D) model both laterally and vertically (cross section). Based on the inversion result that has been conducted, the profile of the average v_S curve, with respect to depth, shows the value of v_S, which increases with increasing depth. At shallow depths (0–5 m), it had an extremely low velocity of less than 330 m/s, indicating that it was composed of soft layers (weathered layers). Hard rock layers (v_S > 1 250 m/s) were visible at depths of > 100 m.

Based on the lateral 2D model, Bandar Lampung City was divided into two rocky zones in the direction of the boundary trending NW-SE. The north-central-eastern part has a higher v_S anomaly, ranging from 30 to 100 m deep. The v_S velocity reached more than 2000 m/s, indicating that the area was dominated by hard rock and thin layers of soft sediment. This is suitable for the dominant frequency anomaly map, which shows that the north-central-eastern region has a high dominant frequency anomaly. This high dominant frequency indicated that the area had a thin layer of sediment. On the south-central-west side, it had a low dominant frequency, which indicates the presence of a thick layer of sediment. Based on the v_S structure map, this area also has low-to-moderate v_S values. Thus, the south-central-west region is a groundwater basin with a sediment layer thickness > 100 m.

These results agree with those of previous studies of groundwater basins at a depth of 800 m. In addition, the v_S structure map shows clear fault structures both laterally and vertically. This was indicated by the difference in contrast between anomalies, both from low-to-moderate and from moderate-to-high anomalies. This fault structure is more clearly observed in the vertical section, where the Bandar Lampung area has a complex fault structure, and many faults are scattered throughout the city. This study provides a clear model description for delineating fault structures, groundwater basin structures, the thickness of weathered layers near the surface, and the characterization of site dynamic parameters, which are needed in seismic hazard and risk reduction studies in urban areas and rapid land use planning. However, more intensive measurements are recommended to obtain better seismic microzonation results.

Conflict of interest

The authors affirm that they have no financial and personal relationships with any individuals or organization that could have potentially influenced the work presented in this paper.

References

Abu Zeid N, Corradini E, Bignardi S, Morandi N, Nizzo V and Santarato G (2016). Unusual geophysical techniques in archaeology - HVSR and induced polarization, A case history. In: Proceedings of the 22nd European Meeting of Environmental and Engineering Geophysics. Barcelona, Spain. https://doi.org/10.3997/2214-4609.201602027.

Abu Zeid N, Bignardi S, Santarato G and Peresani M (2017a). Exploring the paleolithic cave of Fumane (Italy): geophysical methods as planning tool for archaeology. In: Proceedings of the SEG Technical Program Expanded Abstracts 2017. SEG, pp. 5125–5129. https://doi.org/10.1190/segam2017-17729320.1.

Abu Zeid N, Corradini E, Bignardi S, Nizzo V and Santarato G (2017). The passive seismic technique 'HVSR' as a reconnaissance tool for mapping paleo-soils: the case of the *Pilastri* archaeological site, northern Italy. Archaeol Prospect **24**(3): 245–258 https://doi.org/10.1002/arp.1568.

Aki K and Richards PG (2002). Quantitative Seismology. 2nd ed. University Science Books, Sausalito, CA, pp 700.

Akkaya İ (2015). The application of HVSR microtremor survey method in Yüksekova (Hakkari) region, Eastern Turkey. J Afr Earth Sci **109**: 87–95 https://doi.org/10.1016/j.jafrearsci.2015.05.018.

Akkaya İ and Özvan A (2019). Site characterization in the Van settlement (Eastern Turkey) using surface waves and HVSR microtremor methods. J Appl Geophys **160**: 157–170 https://doi.org/10.1016/j.jappgeo.2018.11.009.

Albarello D, Herak M, Lunedei E, Paolucci E and Tanzini A (2023). Simulating H/V spectral ratios (HVSR) of ambient

vibrations: a comparison among numerical models. Geophys J Int **234**(2): 870–878 https://doi.org/10.1093/gji/ggad109.

Asten MW (1978). Geological control on the three-component spectra of rayleigh-wave microseisms. Bull Seismol Soc Am **68**(6): 1 623–1 636 https://doi.org/10.1785/bssa0680061623.

Barber AJ, Crow MJ and Milsom JS (2005). Sumatra: Geology, Resources and Tectonic Evolution. Geological Society Memoir, London, pp 290. https://doi.org/10.1144/gsl.mem.2005.031.

Bignardi S, Abu Zeid N, Corradini E and Santarato G (2017). The HVSR technique from array data, speeding up mapping of paleo-surfaces and buried remains: the case of the Bronze-Age site of Pilastri (Italy). In: Proceedings of the SEG Technical Program Expanded Abstracts 2017. Society of Exploration Geophysicists, pp. 5119–5124. https://doi.org/10.1190/segam2017-17746745.1.

Brocher TM (2005). Empirical relations between elastic wavespeeds and density in the Earth's crust. Bull Seismol Soc Am **95**(6): 2 081–2 092 https://doi.org/10.1785/0120050077.

D'Amico V, Picozzi M, Baliva F and Albarello D (2008). Ambient noise measurements for preliminary site-effects characterization in the Urban Area of Florence, Italy. Bull Seismol Soc Am **98**(3): 1 373–1 388 https://doi.org/10.1785/0120070231.

Dal Moro G (2008). v_S and v_P vertical profiling via joint inversion of Rayleigh waves and refraction travel times by means of bi-objective evolutionary algorithm. J Appl Geophys **66**(1-2): 15–24 https://doi.org/10.1016/j.jappgeo.2008.08.002.

Darmawan IGB, Fahlevi DI, Yassar MF and Pramudya FA (2021). Identifikasi zona reservoar panas bumi berdasarkan analisis fault fracture density Citra digital elevation model ALOS PALSAR di gunung rajabasa. Bul Sumber Daya Geol **16**(2): 119–131 https://doi.org/10.47599/bsdg.v16i2.315.

Ding YM, Zhang WL, Yu L and Lu KH (2019). The accuracy and efficiency of GA and PSO optimization schemes on estimating reaction kinetic parameters of biomass pyrolysis. Energy **176**: 582–588 https://doi.org/10.1016/j.energy.2019.04.030.

European Commission (2004). EN 1998-1:2004 Eurocode 8: Design of structures for earthquake resistance – Part 1:General rules,seismic actions and rules for buildings. European Committee for Standardization (CEN), Brussels, Belgium, pp 34.

Fäh D, Kind F and Giardini D (2003). Inversion of local S-wave velocity structures from average H/V ratios and their use for the estimation of site-effects. J Seismol **7**(4): 449–467 https://doi.org/10.1023/b:jose.0000005712.86058.42.

Farduwin A and Yudistira T (2021). Shear velocity inversion from ambient seismic noise using RR-PSO: A case study of Nusa Tenggara Island. J Phys: Conf Ser **1949**(1): 012 022 https://doi.org/10.1088/1742-6596/1949/1/012022.

Farduwin A, Antosia RM, Putri IA, Santoso NA and Irawati SM (2021). Geoelectrical data inversion using particle swarm optimization: case study of Gayau village. J Geofisika Eksplorasi **7**(2): 88–99 https://doi.org/10.23960/jge.v7i2.118.

Fernández Martínez JL, García Gonzalo E, Fernández Álvarez JP, Kuzma HA and Menéndez Pérez CO (2010). PSO: a powerful algorithm to solve geophysical inverse problems: application to a 1D-DC resistivity case. J Appl Geophys **71**(1): 13–25 https://doi.org/10.1016/j.jappgeo.2010.02.001.

Gallipoli MR, Mucciarelli M, Gallicchio S, Tropeano M and Lizza C (2019). Horizontal to vertical spectral ratio (HVSR) measurements in the area damaged by the 2002 Molise, Italy, Earthquake. Earthquake Spectra **20**(S1): 81–93 https://doi.org/10.1193/1.1766306.

Gutenberg B (1958). Microseisms. Adv Geophys **5**: 53–92 https://doi.org/10.1016/s0065-2687(08)60075-8.

Hamilton WB (1979).Tectonics of the Indonesian region.USGS, Denver, Colorado, 1078: 345.

Hartzell S, Cranswick E, Frankel A, Carver D and Meremonte M (1997). Variability of site response in the Los Angeles urban area. Bull Seismol Soc Am **87**(6): 1 377–1 400 https://doi.org/10.1785/bssa0870061377.

Harutoonian P, Leo CJ, Tokeshi K, Doanh T, Castellaro S, Zou JJ, Liyanapathirana DS and Wong H (2013). Investigation of dynamically compacted ground by HVSR-based approach. Soil Dyn Earthq Eng **46**: 20–29 https://doi.org/10.1016/j.soildyn.2012.12.004.

Herak M (2008). ModelHVSR—A Matlab® tool to model horizontal-to-vertical spectral ratio of ambient noise. Comput Geosci **34**(11): 1 514–1 526 https://doi.org/10.1016/j.cageo.2007.07.009.

Ibs-von Seht M and Wohlenberg J (1999). Microtremor measurements used to map thickness of soft sediments. Bull Seismol Soc Am **89**(1): 250–259 https://doi.org/10.1785/bssa0890010250.

Kawase H, Nagashima F, Nakano K and Mori Y (2019). Direct evaluation of S-wave amplification factors from microtremor H/V ratios: Double empirical corrections to "Nakamura" method. Soil Dyn Earthq Eng **126**: 105 067 https://doi.org/10.1016/j.soildyn.2018.01.049.

Kennedy J and Eberhart R (1995). Particle swarm optimization. In: Proceedings of ICNN'95 - International Conference on Neural Networks, Perth, WA, Australia. Vol.4, pp 1942–1948. https://doi.org/10.1109/ICNN.1995.488968.

Khalili M and Mirzakurdeh AV (2019). Fault detection using microtremor data (HVSR-based approach) and electrical resistivity survey. J Rock Mech Geotech Eng **11**(2): 400–408 https://doi.org/10.1016/j.jrmge.2018.12.003.

Konno K and Ohmachi T (1998). Ground-motion characteristics estimated from spectral ratio between horizontal and vertical components of microtremor. Bull Seismol Soc Am **88**(1): 228–241 https://doi.org/10.1785/bssa0880010228.

Kyaw ZL, Pramumijoyo S, Husein S, Fathani TF and Kiyono J (2015). Seismic behaviors estimation of the shallow and deep soil layers using microtremor recording and EGF technique in Yogyakarta City, central Java Island. Proc Earth Planet Sci **12**: 31–46 https://doi.org/10.1016/j.proeps.2015.03.024.

Lunedei E and Albarello D (2010). Theoretical HVSR curves from full wavefield modelling of ambient vibrations in a weakly dissipative layered Earth. Geophys J Int **181**(2): 1 093–1 108 https://doi.org/10.1111/j.1365-246x.2010.04560.x.

Maghami S, Sohrabi-Bidar A, Bignardi S, Zarean A and Kamalian M (2021). Extracting the shear wave velocity structure of deep alluviums of "Qom" Basin (Iran) employing HVSR inversion of microtremor recordings. J Appl Geophys **185**: 104 246 https://doi.org/10.1016/j.jappgeo.2020.104246.

Mangga SA, Amirudin T, Suwarti S, Gafoer and Sidarto (1993).Geological map of Indonesia quadrangle: Tanjung-karang, Sumatra scale 1:250.000. Geological Research and Development Centre, Bandung.

Mantovani A, Valkaniotis S, Rapti D and Caputo R (2018). Mapping the palaeo-piniada valley, central Greece, based on systematic microtremor analyses. Pure Appl Geophys **175**(3): 865–881 https://doi.org/10.1007/s00024-017-1731-7.

Maresca R, Nardone L, Gizzi FT and Potenza MR (2018). Ambient noise HVSR measurements in the Avellino historical centre and surrounding area (southern Italy). Correlation with surface geology and damage caused by the 1980 Irpinia-Basilicata earthquake. Measurement **130**: 211–222 https://doi.org/10.1016/j.measurement.2018.08.015.

McCaffrey R (2009). The tectonic framework of the Sumatran subduction zone. Annu Rev Earth Planet Sci **37**: 345–366 https://doi.org/10.1146/annurev.earth.031208.100212.

Mihaylov A, El Naggar H, Mihaylov D and Dineva S (2019). Approximate analytical HVSR curve using multiple band-pass filters and potential applications. Soil Dyn Earthq Eng **127**: 105 840 https://doi.org/10.1016/j.soildyn.2019.105840.

Mihaylov D, El Naggar MH and Dineva S (2016). Separation of high-and low-level ambient noise for HVSR: application in city conditions for greater Toronto area. Bull Seismol Soc Am **106**(5): 2 177–2 184 https://doi.org/10.1785/0120150389.

Mucciarelli M and Gallipoli MR (2001). A critical review of 10 years of microtremor HVSR technique. Boll Geofis Teor Appl **42**(3-4): 255–266.

Mulyasari R, Utama HW and Haerudin N (2019). Geomorphology study on the Bandar Lampung Capital City for recommendation of development area. IOP Conf Ser:Earth Environ Sci **279**: 012 026 https://doi.org/10.1088/1755-1315/279/1/012026.

Nakamura Y (1989). A method for dynamic characteristics estimation of subsurface using microtremor on the ground surface. Quart Rep Railway Tech Res Inst **30**(1): 25–33.

Nakamura Y (2000). Clear identification of fundamental idea of Nakamura's technique and its applications.In:Proceedings of the 12th World Conference on Earthquakes Engineering. Auckland, New Zealand, pp 1–8.

Nogoshi M and Igarashi T (1970). On the propagation characteristics of microtremor. Zisin (J Seismol Soc Japan. 2nd Ser.) **23**(4): 264 https://doi.org/10.4294/zisin1948.23.4_264.

Nogoshi M and Igarashi T (1971). On the amplitude characteristics of microtremor (Part 2). Zisin (J Seismol Soc Japan. 2nd Ser.) **24**(1): 26 https://doi.org/10.4294/zisin1948.24.1_26.

Pallero JLG, Fernández-Martínez JL, Bonvalot S and Fudym O (2017). 3D gravity inversion and uncertainty assessment of basement relief via Particle Swarm Optimization. J Appl Geophys **139**: 338–350 https://doi.org/10.1016/j.jappgeo.2017.02.004.

Pamuk E, Akgün M, Özdağ ÖC and Gönenç T (2017). 2D soil and engineering-seismic bedrock modeling of eastern part of Izmir inner bay/Turkey. J Appl Geophys **137**: 104–117 https://doi.org/10.1016/j.jappgeo.2016.12.016.

Panzera F, Halldorsson B and Vogfjörð K (2017). Directional effects of tectonic fractures on ground motion site amplification from earthquake and ambient noise data: A case study in South Iceland. Soil Dyn Earthq Eng **97**: 143–154 https://doi.org/10.1016/j.soildyn.2017.03.024.

Panzera F, Romagnoli G, Tortorici G, D'Amico S, Rizza M and Catalano S (2019). Integrated use of ambient vibrations and geological methods for seismic microzonation. J Appl Geophys **170**: 103 820 https://doi.org/10.1016/j.jappgeo.2019.103820.

Paolucci E, Albarello D, D'Amico S, Lunedei E, Martelli L, Mucciarelli M and Pileggi D (2015). A large scale ambient vibration survey in the area damaged by May–June 2012 seismic sequence in Emilia Romagna, Italy. Bull Earthq Eng **13**(11): 3 187–3 206 https://doi.org/10.1007/s10518-015-9767-5.

Pilz M, Parolai S, Picozzi M, Wang RJ, Leyton F, Campos J and Zschau J (2010). Shear wave velocity model of the Santiago de Chile basin derived from ambient noise measurements: A comparison of proxies for seismic site conditions and amplification. Geophys J Int **182**(1): 355–367 https://doi.org/10.1111/j.1365-246x.2010.04613.x.

Rahman Z, Siddiqua S and Kamal ASMM (2016). Shear wave velocity estimation of the near-surface materials of Chittagong City, Bangladesh for seismic site characterization. J Appl Geophys **134**: 210–225 https://doi.org/10.1016/j.jappgeo.2016.09.006.

Raptakis D and Makra K (2010). Shear wave velocity structure in western Thessaloniki (Greece) using mainly alternative SPAC method. Soil Dyn Earthq Eng **30**(4): 202–214 https://doi.org/10.1016/j.soildyn.2009.10.006.

Rustadi, Darmawan IGB, Haerudin N, Setiawan A and Suharno (2022). Groundwater exploration using integrated geophysics method in hard rock terrains in Mount Betung Western Bandar Lampung, Indonesia. J Ground Sci Eng **10**(1): 10–18 https://doi.org/10.19637/j.cnki.2305-7068.2022.01.002.

Ryanto TA, Iswanto, ER, Indrawati Y, Setiaji AB and Suntoko H (2020). Sediment Thickness estimation in Serpong Experimental Power Reactor Site Using HVSR method. Jurnal Pengembangan Energi Nuklir **22**(1) https://doi.org/10.17146/jpen.2020.22.1.5949.

Scherbaum F, Hinzen KG and Ohrnberger M (2003). Determination of shallow shear wave velocity profiles in the Cologne, Germany area using ambient vibrations. Geophys J

Int **152**(3): 597–612 https://doi.org/10.1046/j.1365-246x.2003.01856.x.

SESAME (2004).Guidelines for the implementation of the H/V spectral ratio technique on ambient vibrations: measurements, processing and interpretation. In: Proceedings of the 13th World Conference on Earthquake Engineering. pp 1–62.

Setiawan B, Jaksa M, Griffith M and Love D (2018). Seismic site classification based on constrained modeling of measured HVSR curve in regolith sites. Soil Dyn Earthq Eng **110**: 244–261 https://doi.org/10.1016/j.soildyn.2017.08.006.

Sieh K and Natawidjaja D (2000). Neotectonics of the Sumatran fault, Indonesia. J Geophys Res: Solid Earth **105**(B12): 28 295–28 326 https://doi.org/10.1029/2000jb900120.

Stanko D, Markušić S, Strelec S and Gazdek M (2017). HVSR analysis of seismic site effects and soil-structure resonance in Varaždin city (North Croatia). Soil Dyn Earthq Eng **92**: 666–677 https://doi.org/10.1016/j.soildyn.2016.10.022.

Sylvette BC, Cécile C, Pierre-Yves B, Fabrice C, Peter M, Jozef K and Fäh D (2006). H/V ratio: a tool for site effects evaluation. Results from 1-D noise simulations. Geophys J Int **167**(2): 827–837 https://doi.org/10.1111/j.1365-246x.2006.03154.x.

Toni M, Yokoi T and El Rayess M (2019). Site characterization using passive seismic techniques: a case of Suez city, Egypt. J Afr Earth Sci **156**: 1–11 https://doi.org/10.1016/j.jafrearsci.2019.05.004.

Wilken D, Wunderlich T, Majchczack B andersen J and Rabbel W (2015). Rayleigh-wave resonance analysis: a methodological test on a Viking age pit house. Archaeol Prospect **22**(3): 187–206 https://doi.org/10.1002/arp.1508.

Zaenudin A, Risman R, Darmawan IGB and Yogi IBS (2020). Analysis of gravity anomaly for groundwater basin in Bandar Lampung city based on 2D gravity modeling. J Phys:Conf Ser **1572**: 012 006 https://doi.org/10.1088/1742-6596/1572/1/012006.

Zaenudin A, Darmawan IGB, Farduwin A, and Wibowo RC. (2022). Shear wave velocity estimation based on the particle swarm optimization method of HVSR curve inversion in Bakauheni district, Indonesia. Turkish Journal of Earth Sciences 31(5): Article 5 https://doi.org/10.55730/1300-0985.1815.